histograms needed to arithmetic encode the quantizer indexes. Such an arithmetic coding achieves rates equal to or slightly more than the zeroth-order entropy of its input, so no additional compression has been achieved by arithmetic coding in our simulations. The possible advantage of an adaptive arithmetic code needs to be studied.

For the *Lena* image, average bit rates versus peak-signal to rms-noise-ratios (PSNR's) for different schemes are plotted in Fig. 6. The bit rate includes all the information necessary to decode the image. In this plot, we compare the four-class subband FSSQ with five other techniques. The one-class subband FSSQ refers to the case where all the pixels of a subband belong to a single class and is equivalent to a simple 10-subband coding scheme with scalar quantizers. The [T. & F.], [Y.H.K.], [M. & N.], [J.M.S.] and [J. et al.] results in this plot are taken from [1], [2], [4], [6] and [7], respectively. Note that the results in [M. & N.] and [J. et al.] could be improved by use of variable-length coding. Our subband-FSSQ technique gave a better performance than the other subband coding techniques at higher bit rates. At an average rate of 1.0 b/pixel, the subband-FSSQ resulted in a 3% reduction in the quantization noise compared to other techniques. The *Lena* encoded at 0.65 b/pixel is shown in Fig. 7.

In general, motion-compensated coding techniques provide the best compression for video. However, in certain video processing applications such as digital video effects, motion-compensated coding of video may not be applicable. For such applications, intraframe coding, e.g., subband FSSQ, is preferred. Performances of four-class subband FSSQ and one-class subband FSSQ on a *MIT* HD video are compared in Fig. 8. In this plot, we see that at an average rate of 1.0 b/pixel, the four-class subband FSSQ gives a 29.1% reduction in quantizer noise with respect to the one-class subband FSSQ, or, equivalently, a 13.6% reduction in the bit rate to achieve a PSNR of 37 dB. Performance of four-class subband FSSQ on a frame-by-frame basis on this video at an average bit rate of 0.77 b/pixel is shown in Fig. 9.

From above coding results on a still image and an HD video, we conclude that the subband-FSSQ algorithm was successful in exploiting the energy correlation between the spatial subbands of real-life images and videos. A vector version of this algorithm using lattice quantizers could provide further exploitation of this correlation.

The subband-FSSQ algorithm is simple enough to be implementable in real time. For the 512×512 monochrome *Lena*, the splitting took 9.8 s on a Sun 4/75 workstation. The first pass that includes gathering of statistics and bit allocation took 6.6 s. This does not include the time needed to fit GG models. The second pass that performs actual quantization, arithmetic coding, arithmetic decoding, and the synthesis of encoded subbands took 37.1 s. Thus, encoding and decoding together, excluding the time to fit GG models, took 53.5 s. While we used the CPU-intensive Kolmogorov–Smirnov test [14] to fit GG models, other much faster methods such as the one given in [15] should work just as well.

REFERENCES

[1] N. Tanabe and N. Farvardin, "Subband image coding using entropy-coded quantization over noisy channels," *J. Select. Areas Commun.*, vol. 10, no. 5, pp. 926–943, June 1992.

[2] Y. H. Kim and J. W. Modestino, "Adaptive entropy coded subband coding of images," *IEEE Trans. Image Processing*, vol. 1, no. 1, pp. 31–48, Jan. 1992.

[3] A. Pentland and B. Horowitz, "A practical approach to fractal-based image compression," in *Proc. SPIE Conf. Visual Commun. Image Processing*, vol. 1605, Nov. 1991, pp. 467–474.

[4] N. Mohsenian and N. M. Nasrabadi, "An edge-based subband image coding technique for encoding the upper frequency bands," in *Proc. SPIE Conf. Visual Commun. Image Processing*, vol. 1605, Nov. 1991, pp. 781–791.

[5] T. Naveen and J. W. Woods, "Subband finite state scalar quantization," in *Proc. IEEE ICASSP*, vol. v, 1993, pp. 613–616.

[6] J. M. Shapiro, "Embedded image coding using zerotrees of wavelet coefficients," *IEEE Trans. Signal Processing*, vol. 41, no. 12, pp. 3445–3462, Dec. 1993.

[7] O. Johnsen, O. V. Shentov, and S. K. Mitra, "A technique for the efficient coding of the upper bands in subband coding of images," in *Proc. IEEE ICASSP*, 1990, pp. 2097–2100.

[8] A. Gersho and R. M. Gray, "Finite-state vector quantization," in *Vector Quantization and Signal Compression*. Norwell, MA: Kluwer, 1992, pp. 431–459.

[9] N. Farvardin and J. W. Modestino, "Optimum quantizer performance for a class of non-Gaussian memoryless sources," *IEEE Trans. Inform. Theory*, vol. IT-30, no. 3, pp. 485–497, May 1984.

[10] N. S. Jayant and P. Noll, *Digital Coding of Waveforms*. Englewood Cliffs, NJ: Prentice–Hall, 1984.

[11] J. G. Ecker and M. Kupferschmid, "Nonlinear programming," in *Introduction to Operations Research*. Malabar, FL: Krieger, 1991.

[12] B. Mahesh and W. A. Pearlman, "Image coding on a hexagonal pyramid with noise spectrum shaping," in *Proc. SPIE Conf. Visual Commun. Image Processing IV*, vol. 1199, Nov. 1989, pp. 764–774.

[13] C. B. Jones, "An efficient coding system for long source sequences," *IEEE Trans. Inform. Theory*, vol. IT-27, pp. 280–291, May 1981.

[14] P. H. Westerink, "Subband coding of images," Ph.D. dissertation, Delft Univ. of Technol., The Netherlands, 1989.

[15] S. G. Mallat, "A theory for multiresolution signal decomposition: The wavelet representation," *IEEE Trans. Patt. Anal. Machine Intell.*, vol. 11, no. 7, pp. 674–693, July 1989.

The Design of Two-Dimensional Gradient Estimators Based on One-Dimensional Operators

M. Azaria, I. Vitsnudel, and Y. Y. Zeevi

***Abstract*— A computational procedure for the extension of one-dimensional (1-D) gradient estimators to two dimensions (2-D) is presented. The procedure is equivalent to the surface fitting method. It is, however, simpler in design, as the design is 1-D rather than 2-D. Higher order derivative estimators can also be constructed by the same procedure.**

I. INTRODUCTION

Two-dimensional (2-D) gradient estimators are some of the most useful tools in image processing. The basic approach for their construction is the surface fitting method, which fits a surface to the data of an image window. This approach was introduced by Prewitt [1] who, assuming quadratic surfaces, constructed 3×3 and 4×4 masks. Haralick [2] was one of the first to stress the need to consider larger supports and introduced the Facet model, modeling surfaces of edges by cubic surfaces. Poggio *et al.* [3] proposed a 2-D surface fitting scheme based on generalized cubic splines.

Manuscript received April 8, 1994; revised April 12, 1995. This research was supported by the Ollendorff Center, the Israel Science Foundation, and by the Fund for the Promotion of Research at the Technion. The associate editor coordinating the review of this paper and approving it for publication was Nikolas P. Galatsanos.

The authors are with the Department of Electrical Engineering Technion—Israel Institute of Technology, Haifa, Israel.

Publisher Item Identifier S 1057-7149(96)00143-1.

We present an equivalent approach to the surface fitting method that is most suitable for construction of large support masks, which is based on one-dimensional (1-D) design rather than 2-D design. The 1-D design allows a simpler and yet detailed construction of these masks.

This correspondence is organized as follows: In Section II, we present our computational procedure for the construction of 2-D gradient masks. In Section III, we describe the derivation of the 1-D estimators we use. In Section IV, we construct two 7×7 masks: GRD7 and RAMP7 using our procedure, and compare their performances with the popular gradient of Gaussian mask [4]. In Section V, we summarize our work and point directions for further research.

II. The Interpolation Kernel

The design procedure consists of three computational stages:

A. Data Transformation: Resampling

At this stage, we resample the $N \times N$ image data matrix ϕ to obtain a form that is more convenient for our processing.

The image data is resampled along P symmetric rays emanating from the center, where each ray contains Q points. The resampling is implemented by applying a linear interpolation transformation (for which we use 2-D cubic splines). The value of the interpolated sample point ϕ'_{ij} is given by

$$\phi'_{ij} = \sum_{\alpha=1}^{N}\sum_{\beta=1}^{N} R_{ij\alpha\beta}\phi_{\alpha\beta} \quad \begin{matrix} i = 1, P \\ j = 1, Q \end{matrix} \tag{2.1}$$

where i denotes the ray number, and j is the number of point.

We call the 4-D interpolation matrix $R_{P\times Q\times N\times N}$ the interpolation kernel. The value $R_{ij\alpha\beta}$ is the impulse response of a 2-D interpolation filter $H_{ij}^{(2)}(\alpha,\beta)$ designed to interpolate at the resampled grid point (i,j). Thus

$$R_{ij\alpha\beta} = H_{ij}^{(2)}(\alpha,\beta). \tag{2.2}$$

B. 1-D Derivative Estimation

Having transformed our data into a convenient form to process, we now apply our 1-D operator. For our purpose, we apply linear 1-D derivative estimators to each of the P rays.

The form of the 1-D derivative estimator depends on the signal-to-noise ratio and on signal design considerations. In Section III, we sketch a simple derivation of the derivative estimators we use.

In general, one applies different operators D^i (or the same operator with different weighting) to each of the rays to obtain the estimated value $\hat{d}_i$ of the orientational derivative of the ith ray. Note that for derivative estimators, different weightings should be used to account for different length scales at different orientations. Thus

$$\hat{d}_i = \sum_{j=1}^{Q} D_j^i \cdot \phi'_{ij} \qquad i = 1, P. \tag{2.3}$$

(One can also introduce directional considerations in this way).

C. Parameter Extraction by the Least Squares Procedure

In general, one introduces redundancy by processing more data samples than needed to fix the estimated parameters. This is done to reduce the effects of noise and thus obtain better estimates. Specifically, for our application, note the relation that exists between the orientational derivative of ray i $\hat{d}_i = \frac{\partial\phi}{\partial n_i}$ and the 2-D gradient $\left(\frac{\widehat{\partial\phi}}{\partial x}, \frac{\widehat{\partial\phi}}{\partial y}\right)$ to be estimated

$$\hat{d}_i = \frac{\partial\phi}{\partial n_i} = n_x^i \frac{\widehat{\partial\phi}}{\partial x} + n_y^i \frac{\widehat{\partial\phi}}{\partial y} \qquad i = 1, P \tag{2.4}$$

where n_x^i and n_y^i are the cosines of orientation of ray i. Applying the least squares procedure and assuming that a symmetric choice of ray orientiations has been taken results in the following estimates:

$$\begin{aligned} \frac{\widehat{\partial\phi}}{\partial x} &= C_P \sum_{i=1}^{P} \hat{d}_i n_x^i \\ \frac{\widehat{\partial\phi}}{\partial y} &= C_P \sum_{i=1}^{P} \hat{d}_i n_y^i \end{aligned} \tag{2.5}$$

where C_P is a normalization constant given by

$$C_P = \frac{1}{\sum_{i=1}^{P} n_x^{i^2}} = \frac{1}{\sum_{i=1}^{P} n_y^{i^2}}. \tag{2.6}$$

Rewriting (2.5) by inserting (2.1) and (2.3), we get for $\frac{\widehat{\partial\phi}}{\partial x}$

$$\begin{aligned} \frac{\widehat{\partial\phi}}{\partial x} &= C_P \sum_{i=1}^{P}\sum_{j=1}^{Q}\sum_{\alpha=1}^{N}\sum_{\beta=1}^{N} n_x^i D_j^i R_{ij\alpha\beta}\phi_{\alpha\beta} \\ &= \sum_{\alpha=1}^{N}\sum_{\beta=1}^{N}\left(C_P \sum_{i=1}^{P}\sum_{j=1}^{Q} n_x^i D_j^i R_{ij\alpha\beta}\right)\phi_{\alpha\beta} \\ &= \sum_{\alpha=1}^{N}\sum_{\beta=1}^{N} W_{\alpha\beta}^x \phi_{\alpha\beta} \end{aligned} \tag{2.7}$$

where $W_{\alpha\beta}^x$ is defined by

$$W_{\alpha\beta}^x = C_P \sum_{i=1}^{P}\sum_{j=1}^{Q} n_x^i D_j^i R_{ij\alpha\beta} \qquad \alpha = 1, N; \beta = 1, N \tag{2.8}$$

and similarly for $\frac{\widehat{\partial\phi}}{\partial y}$

$$W_{\alpha\beta}^y = C_P \sum_{i=1}^{P}\sum_{j=1}^{Q} n_y^i D_j^i R_{ij\alpha\beta} \qquad \alpha = 1, N; \beta = 1, N. \tag{2.9}$$

The masks W^x and W^y of dimensions $N \times N$ are our final result as the x and y components of the estimators of the 2-D gradient.

Derivation of second-order operators can also be accomplished by a similar sequence of operations.

Consider, for example, the derivation of estimators (masks) $W^{(2)x}, W^{(2)y}$ for $\frac{\widehat{\partial^2\phi}}{\partial x^2}$ and $\frac{\widehat{\partial^2\phi}}{\partial y^2}$.

Applying 1-D estimators for the second derivative $D^{(2)i}$ results in the estimate $\hat{d}_i^{(2)}$. Using (2.4) in its operator form yields

$$\hat{d}_i^{(2)} = \frac{\partial^2\phi}{\partial n_i^2} = n_x^{i^2}\frac{\widehat{\partial^2\phi}}{\partial x^2} + n_y^{i^2}\frac{\widehat{\partial^2\phi}}{\partial y^2} + 2n_x^i n_y^i \frac{\widehat{\partial^2\phi}}{\partial x\partial y} \qquad i = 1, P. \tag{2.10}$$

Applying the least squares procedure (where symmetric choice of orientations is assumed) and interchanging the order of summation as in (2.7) yields the following estimators:

$$\begin{aligned} W_{\alpha\beta}^{(2)x} &= \sum_{i=1}^{P}\sum_{j=1}^{Q}\left(n_x^{i^2}\cdot c_1 - n_y^{i^2}\cdot c_2\right) D_j^{(2)i} R_{ij\alpha\beta} \\ &\qquad a = 1, N; \beta = 1, N \\ W_{\alpha\beta}^{(2)y} &= \sum_{i=1}^{P}\sum_{j=1}^{Q}\left(n_y^{i^2}\cdot c_1 - n_x^{i^2}\cdot c_2\right) D_j^{(2)i} R_{ij\alpha\beta} \end{aligned} \tag{2.11}$$

where the constants c_1 and c_2 are given by

$$c_1 = \sum_{i=1}^{P} n_x^{i^4} \Big/ \left(\left(\sum_{i=1}^{P} n_x^{i^4} \right)^2 - \left(\sum_{i=1}^{P} n_x^{i^2} n_y^{i^2} \right)^2 \right)$$

$$c_2 = \sum_{i=1}^{P} n_x^{i^2} n_y^{i^2} \Big/ \left(\left(\sum_{i=1}^{P} n_x^{i^4} \right)^2 - \left(\sum_{i=1}^{P} n_x^{i^2} n_y^{i^2} \right)^2 \right). \quad (2.12)$$

III. Derivation of 1-D Derivative Estimators

We outline here the derivation of the 1-D gradient (derivative) estimators designed for the case of $Q = 7$ data samples.

Let us assume that the signal waveforms under consideration are well approximated by polynomials of order 4 in a seven-sample support $t = -3, -2, -1, 0, 1, 2, 3$ (unit scale assumed).

The signal waveforms are corrupted by additive white Gaussian noise $n(t)$ with zero mean and variance σ^2. The signal waveforms can be decomposed into a sum of even and odd components:

$$s(t) = (d_0 + d_2 \cdot t^2 + d_4 t^4) + (d_1 t + d_3 t^3). \quad (3.1)$$

Since we wish to estimate the coefficient d_1, the even component is irrelevant. Hence, we take our derivative estimator as a linear antisymmetric filter $w(t)$ (the optimal estimator in the sense of mean squares error for Gaussian noise is the linear filter)

$$w(t) = (-\gamma, -\beta, -\alpha, 0, \alpha, \beta, \gamma). \quad (3.2)$$

Our estimate $\hat{d}_1$ thus reads

$$\begin{aligned} \hat{d}_1 &= \textstyle\sum_{t=-3}^{3} w(t) \cdot [s(t) + n(t)] \\ &= d_1 \cdot (2\alpha + 4\beta + 6\gamma) + d_3 \cdot (2\alpha + 16\beta + 54\gamma) + \tilde{n}(t) \end{aligned} \quad (3.3)$$

where $\tilde{n}(t) = -\gamma n(-3) - \beta n(-2) - \alpha n(-1) + \alpha n(1) + \beta n(2) + \gamma n(3)$ is zero mean Gaussian noise with variance $2(\alpha^2 + \beta^2 + \gamma^2)\sigma^2$.

It is clear from (3.3) that the optimal unbiased estimator should satisfy three constraints:

$$\text{The coefficient of } d_1 \text{ should be taken as 1, i.e., } 2\alpha + 4\beta + 6\gamma = 1. \quad (3.4)$$

$$\text{The coefficient of } d_3 \text{ should be taken as 0, i.e., } 2\alpha + 16\beta + 54\gamma = 0 \quad (3.5)$$

and the variance of $\tilde{n}(t)$ should be minimized, i.e.

$$\text{minimize} \quad 2\sigma^2 \cdot (\alpha^2 + \beta^2 + \gamma^2). \quad (3.6)$$

Solving (3.4)–(3.6) renders the 1-D derivative estimator GRD7 with coefficients $\alpha = \frac{58}{252}$, $\beta = \frac{67}{252}$, and $\gamma = \frac{-22}{252}$.

When better noise suppression performance is required, biased estimators should be used. For example, when one ignores the cubic term, the resultant filter is RAMP7: $\alpha = \frac{1}{28}$, $\beta = \frac{2}{28}$, $\gamma = \frac{3}{28}$.

For the case of five-sample support, the estimator $[-\beta, -\alpha, 0, \alpha, \beta]$ is a two-parameter filter. Hence, it is impossible to design an unbiased estimator, which will satisfy all three constraints (3.4)–(3.6).

When one ignores the noise, the filter parameters are $\alpha = \frac{2}{3}$, $\beta = -\frac{1}{12}$. This filter is well known from numerical analysis.

When one ignores the cubic term, the filter parameters are $\alpha = \frac{1}{10}$ and $\beta = \frac{1}{5}$. This RAMP5 filter is also known from numerical analysis [6].

IV. An Example

We construct two 7×7 masks: RAMP7 and GRD7. These masks use 16 orientations. RAMP7 is a planar mask based on the 1-D derivative estimator $\frac{1}{28}(-3, -2, -1, 0, 1, 2, 3)$. GRD7 uses the 1-D filter $\frac{1}{252}(22, -67, -58, 0, 58, 67, -22)$ and constitutes an unbiased estimator for cubic surfaces. The noise reduction gain of RAMP7 is -21.9dB, and that of GRD7 is -11.3dB. (The noise reduction gain of the 3×3 Sobel is -7.3 dB). The GRD7 mask is useful only for high values of SNR. The price required to achieve the cubic term cancellation capability of GRD7 is a decrease in its noise reduction capability. The GRD7 mask is

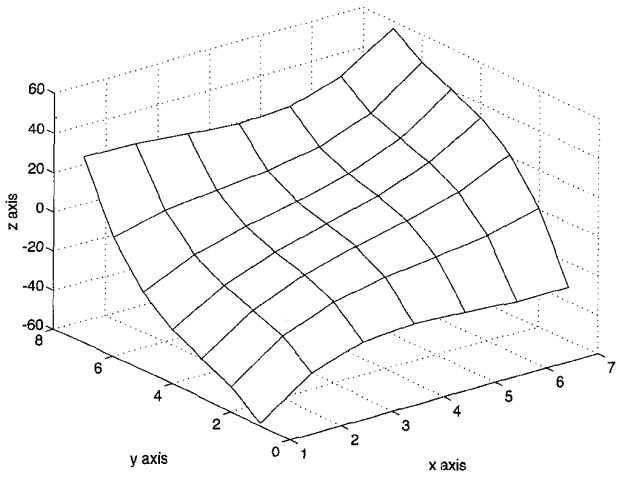

Fig. 1. Example to the test surface.

$$W_x^{GRD7} = 10^{-4} \begin{bmatrix} 49 & 76 & 55 & 0 & -55 & -76 & -49 \\ 121 & -243 & -301 & 0 & 301 & 243 & -121 \\ 156 & -639 & -685 & 0 & 685 & 639 & -156 \\ 81 & -490 & -1138 & 0 & 1138 & 490 & -81 \\ 156 & -639 & -685 & 0 & 685 & 639 & -156 \\ 121 & -243 & -301 & 0 & 301 & 243 & -121 \\ 49 & 76 & 55 & 0 & -55 & -76 & -49 \end{bmatrix}. \quad (4.1)$$

The performances of the GRD7 and RAMP7 masks are compared with those of three gradient estimators of the Gaussian masks (with $\sigma = 1, 2, 3$) constructed by Canny's scheme [4].

The masks were tested by simulation on a 7×7 cubic surface (Fig. 1) constructed by means of the formula

$$\phi_c(x, y) = c\Big[(k_L \cos\phi)x + (k_L \sin\phi)y + k_{xy}xy + k_{x^2y}x^2y + k_{y^2x}y^2x + k_{x^3}x^3 + k_{y^3}y^3\Big]$$

where the parameter k_L controls the planarity of the surface, and c is an appropriate normalization factor. The results of simulations in which the azimuth and magnitude of the gradient were estimated are summarized in Tables I and II. The mean squared error (MSE) of the azimuth of the estimated gradient is given in degrees. The MSE of the amplitude of the estimated gradient is normalized by its exact value and is given in percent. The results are given for

$$k_L = 8, 20, 120,\ k_{xy} = -0.123,\ k_{x^2y} = 0.567,$$

$$k_{y^2x} = -0.789,\ k_{x^3} = 0.456,\ k_{y^3} = 0.678.$$

The azimuth of the gradient ϕ is randomly selected in the range $(-90°, +90°)$.

The results of simulations clearly exhibit the superiority of the GRD7 mask over RAMP7 and the Gaussian masks at the high SNR region. As the SNR drops below 20 dB, the performance of GRD7 degrades significantly due to its lower noise reduction gain. Note that the failure of the planar mask RAMP7 and the Gaussian masks at cubic surfaces is inherent in their structure. These masks will *always*

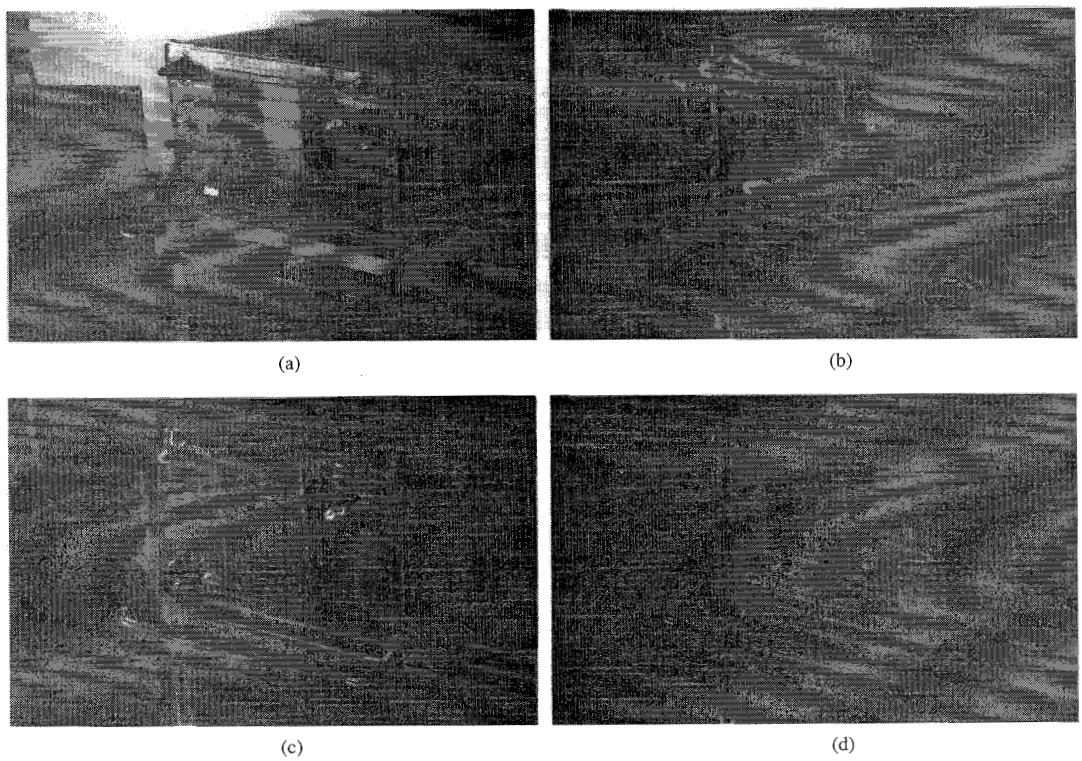

(a) (b) (c) (d)

Fig. 2. Comparison of gradient maps produced by three masks: (a) Image; (b) gradient map estimated by Ramp7; (c) gradient map estimated by Gauss1; (d) gradient map estimated by GRD7.

TABLE I
AZIMUTH MSE (IN DEGREES) FOR GRADIENT ESTIMATORS VS SNR (IN DECIBELS): (a) Cubic surface $k_L = 8$; (b) cubic surface $k_L = 20$; (c) cubic surface $k_L = 120$

SNR dB	GRD7	RAMP7	GAUSS $\sigma = 1$	GAUSS $\sigma = 2$	GAUSS $\sigma = 3$	3 × 3 Sobel
30	3°	33.2°	93.3°	69.1°	47.3°	6.6°
20	5.4°	33.2°	93.3°	69.1°	47.4°	9°
15	8.9°	33.3°	93.3°	69.4°	47.7°	13.5°
10	16.2°	33.5°	93.6°	69.6°	48.5°	24.2°
5	35.8°	34.1°	93.8°	70.4°	49.7°	46.6°
0	61.3°	36°	94.1°	70.8°	55.4°	73.5°

(a)

SNR dB	GRD7	RAMP7	GAUSS $\sigma = 1$	GAUSS $\sigma = 2$	GAUSS $\sigma = 3$	3 × 3 Sobel
30	1.8°	12.3°	23.6°	17.7°	15.9°	3.3°
20	3.9°	12.3°	23.7°	17.8°	16°	5.8°
15	6.6°	12.6°	24°	18°	16.2°	9.9°
10	11.8°	12.9°	24.8°	18.4°	16.5°	17°
5	21.8°	13.8°	26.6°	19.3°	17.3°	35°
0	48.9°	16.2°	32°	21.5°	19.2°	63.3°

(b)

SNR dB	GRD7	RAMP7	GAUSS $\sigma = 1$	GAUSS $\sigma = 2$	GAUSS $\sigma = 3$	3 × 3 Sobel
30	1.3°	2.1°	3.8°	2.9°	2.7°	2.1°
20	3.6°	2.3°	4.2°	3.1°	2.8°	5.4°
15	6°	2.7°	4.9°	3.5°	3.1°	9.1°
10	10.9°	3.7°	6.7°	4.3°	3.9°	16.6°
5	19.7°	5.8°	10.5°	6.3°	5.6°	32.4°
0	42°	9.7°	18.8°	10.1°	8.9°	67°

(c)

TABLE II
AMPLITUDE MSE (IN PERCENT) FOR GRADIENT ESTIMATORS VS SNR (IN DECIBELS): (a) Cubic surface $k_L = 8$; (b) cubic surface $k_L = 20$; (c) cubic surface $k_L = 120$

SNR dB	GRD7	RAMP7	GAUSS $\sigma = 1$	GAUSS $\sigma = 2$	GAUSS $\sigma = 3$	3 × 3 Sobel
30	4.4%	48.8%	75.9%	66.0%	61.4%	11.2%
20	8.0%	48.8%	75.9%	65.8%	61.4%	14.0%
15	13.3%	48.9%	75.9%	66.0%	61.4%	21.6%
10	22.8%	49.3%	76.1%	66.0%	61.6%	36.3%
5	38.5%	50.2%	77.8%	66.4%	62.1%	60.2%
0	67.9%	53.3%	83.8%	68.4%	63.6%	111.4%

(a)

SNR dB	GRD7	RAMP7	GAUSS $\sigma = 1$	GAUSS $\sigma = 2$	GAUSS $\sigma = 3$	3 × 3 Sobel
30	2.9%	19.0%	34.7%	26.9%	24.3%	5.6%
20	5.5%	19.0%	34.5%	26.8%	24.3%	8.9%
15	9.5%	19.2%	34.8%	27.0%	24.5%	15.0%
10	16.2%	19.6%	35.2%	27.2%	24.7%	25.7%
5	28.1%	20.7%	36.9%	28.0%	25.4%	43.0%
0	48.3%	23.8%	41.8%	30.2%	27.5%	75.2%

(b)

SNR dB	GRD7	RAMP7	GAUSS $\sigma = 1$	GAUSS $\sigma = 2$	GAUSS $\sigma = 3$	3 × 3 Sobel
30	1.9%	3.0%	5.5%	4.2%	3.8%	2.9%
20	4.6%	3.2%	5.9%	4.4%	4.0%	7.0%
15	8.0%	3.7%	6.7%	4.8%	4.3%	12.2%
10	13.8%	4.9%	8.7%	5.8%	5.2%	21.3%
5	23.7%	7.4%	13.2%	8.2%	7.4%	36.9%
0	41.2%	12.4%	22.1%	13.1%	11.8%	63.8%

(c)

fail (no matter what size of support is considered) whenever there are significant cubic terms. On the other hand, when one considers larger supports (9×9 or 11×11), it is possible to design by means of our procedure masks that will exhibit good performance in two respects: accuracy and immunity to noise. (Immunity to noise is also needed in order to suppress "model noise" caused by deviations of the surface from the assumed model).

Fig. 2(b)–(d) displays the raw gradient maps (i.e., gradient magnitude without thresholding) produced by the masks RAMP7, Gauss1, and GRD7 operating on the noiseless image of Fig. 2(a). It is shown that the edges produced by GRD7 are relatively thinner, which implies that this type of a mask should be used in an edge detection scheme at the high SNR region. We emphasize, however, that our goal in this correspondence is the design of gradient estimators and

not of edge detectors. Gradient estimators are only one component used by an edge detection scheme [5].

V. Conclusions

We have presented a new approach for the construction of 2-D gradient estimators. The procedure is equivalent to the surface fitting method. It is, however, simpler in design as the design is based on a 1-D operator rather than on a 2-D one. Further work lies in a detailed analysis as well as experimentation with the masks produced by the procedure. Higher order derivative estimators can be also constructed using the same procedure.

Acknowledgment

The authors wish to thank the reviewers for some useful remarks and suggestions.

References

[1] J. M. S. Prewitt, "Object enhancement and extraction," *Picture Processing and Psychopictorics*, B. S. Lipkin and A. Rosenfeld, Eds. New York: Academic, 1970, pp. 75–149.
[2] R. M. Haralick, "Edge and region analysis for digital image data," *Comput. Graphics Image Processing*, vol. 12, pp. 60–73, 1980.
[3] T. Poggio, H. Voorhees, and A. Yuille, "A regularized solution to edge detection," *J. Complexity*, vol. 4, pp. 106–123, 1984.
[4] J. Canny, "A computational approach to edge detection", *IEEE Trans. Patt. Anal. Machine Intell.*, vol. PAMI-8, no. 6, pp. 679–697, Nov. 1986.
[5] M. M. Fleck, "Multiple widths yield reliable finite differences," *IEEE Trans. Patt. Anal. Machine Intell.*, vol. 14, no. 4, Apr. 1992.
[6] F. Scheid, *Numerical Analysis*, Schaum Outline Series. New York: McGraw-Hill, 1969.

Identification of Image and Blue Parameters in Frequency Domain Using the EM Algorithm

Emin Anarim, Hakan Uçar, and Yorgo Istefanopulos

***Abstract*—In this correspondence, we extend the method presented in a recent paper, which considers the problem of the semicausal autoregressive (AR) parameter identification for images degraded by observation noise only. We propose a new approach to identify both the causal and semicausal AR parameters and blur parameters without *a priori* knowledge of the observation noise power and the PSF of the degradation. We decompose the image into 1-D independent complex scalar subsystems resulting from the vector state-space model by using the unitary discrete Fourier transform (DFT). Then, by applying the expectation-maximization (EM) algorithm to each subsystem, we identify the AR model and blur parameters of the transformed image. The AR parameters of the original image are then identified by using the least squares (LS) method. The restored image is obtained as a byproduct of the EM algorithm.**

Manuscript received August 8, 1993; revised December 21, 1994. This work was supported by both TÜBİTAK under contract EEEAG-139 and Boğaziçi University Research Foundation under contract 94A0238. This work was partly presented MELECON-94, Turkey. The associate editor coordinating the review of this paper and approving it for publication was Prof. Xinhua Zhuang.

The authors are with Boğaziçi University, Department of Electrical and Electronics Engineering, Istanbul, Turkey.

Publisher Item Identifier S 1057-7149(96)01143-8.

I. Introduction

Restoration of images distorted by a system with a blur function has been studied by several researchers in recent years [1]–[22]. Usually, due to the imperfections in the electronic, photographic, or transmission medium, the image model identification has to be performed in the presence of observation noise and blur. The classical approaches in the literature assume that the power of the observation noise and some knowledge about the point spread function (PSF) of blur are known *a priori* and only with this assumption does identification become possible. Otherwise, image identification techniques generally requires the optimization of a highly complicated function. In order to avoid complexity of the identification problem, recently, the EM algorithm was proposed for simultaneous restoration and identification of noisy blurred images without knowing the degradation parameters and image statistics *a priori* [1]–[4].

This paper is an extension of the work carried by Lagendijk in 1990 [2], [3] and later by Katayama and Hirai in 1990 [1], and Yemez *et al.* in 1993 [4]. In [3], Lagendijk applied the EM algorithm to the maximum likelihood (ML) image identification problem for images degraded by both blur and noise. In this respect, the identification of the 2-D causal AR model parameters is required. By making use of the EM algorithm, the method can identify the causal AR models without *a priori* knowledge of the observation noise; however, the computational load is excessive due to the 2-D structure of images. Then, in [1], Katayama and Hirai proposed reduction of dimensionality of the 2-D system equations into 1-D case for images degreaded by noise only by the use of the discrete sine transform (DST), as proposed originally by Jain [23]. Next, Yemez *et al.* investigated the same problem but they have used the discrete fourier transform (DFT) instead of the DST. In this study, decomposition of 2-D system equations representing the image into 1-D scalar subsystems using the DFT suggested in [4] has been applied to the general system equations which include both observation noise and blur.

II. Image Representation and AR Modeling

Here, we consider a monochromatic image of size $N \times N$ pixels and denote the gray levels of the original image and the observed image by $x(n, m)$ and $y(n, m)$, respectively, where m is the vertical and n is the horizontal position variable. To model the image, we use the following 2-D AR model, driven by a zero mean random model noise $w(n, m)$:

$$x(n, m) = \sum_{k,l \in S} a_{kl} x(n-k, m-l) + w(n, m) \qquad (1)$$

where $\{a_{kl}\}$ denote the image model coefficients that are determined by minimizing the variance of the noise $\sigma_w^2 = E[w^2(n, m)]$. In (1), S stands for the image model support. Different selection of support regions results in different models. Since use of the nonsymmetric half-plane (NSHP) model elimiantes the necessity of delaying the observations for a 2-D recursion and assures stability [24], the NSHP causal model support is selected for image representation. However, the proposed technique can also be applied to the both quarter-plane (QP) and semicausal models as well.

Based on the linear and spatially invariant (LSI) assumption, the model for the blurred image can be given as

$$y(n, m) = \sum_{k,l \in S_1} d(k, l) x(n-k, m-l) \qquad (2)$$